Investigation of the overvoltage and fast transient phenomena on transformer terminals by taking into account the grounding effects

Popov, M; Grcev, L; Høidalen, KR

DOI
10.1109/TIA.2015.2411652

Publication date
2015

Document Version
Final published version

Published in
IEEE Transactions on Industry Applications

Investigation of the Overvoltage and Fast Transient Phenomena on Transformer Terminals by Taking Into Account the Grounding Effects

Marjan Popov, *Senior Member, IEEE*, Leonid Grcev, *Fellow, IEEE*, Hans Kr. Høidalen, *Senior Member, IEEE*, Bjørn Gustavsen, *Fellow, IEEE*, and Vladimir Terzija, *Senior Member, IEEE*

***Abstract*—A large number of electromagnetic transient studies have so far reported findings related to the overvoltage behavior of systems within a broad frequency range. However, in most cases, actual grounding effects have been either not taken into account or have been just partially considered. Although an accurate methodology to study grounding effects exists, a detailed analysis of the grounding effects has not yet been fully performed. Moreover, many test applications are performed in laboratories where the grounding is close to ideal. In this paper, the grounding system modeling methodology is described, and its capability is demonstrated for an existing complex grounding system. First, the complex grounding system is modeled in the frequency domain by the TRAGSYS program, which represents the grounding system as an equivalent multiport network. Next, the equivalent network parameters are represented in a broad frequency range enabling time domain computations in ATP-EMTP. Finally, the protection level of the chosen lightning arresters is discussed under most severe conditions.**

***Index Terms*—ATP-EMTP, electromagnetic modeling, grounding, lightning arresters, protection, transformers, transients.**

NOMENCLATURE

m, n	Segments in the grounding mesh.
I_n	Current in a specific segment of the grounding mesh.
U_n	Induced voltage in the nth segment.
Z_{Smn}	Mutual impedance between nodes m and n.
D, E $\underline{c}_n$, $\underline{a}_n$	Parameters of the polynomial expression.

Manuscript received December 23, 2014; accepted February 25, 2015. Date of publication March 11, 2015; date of current version November 18, 2015. Paper 2014-PSEC-0910, approved for publication in the IEEE TRANSACTIONS ON INDUSTRY APPLICATIONS by the Power Systems Engineering Committee of the IEEE Industry Applications Society.

M. Popov is with the Faculty of Electrical Engineering, Mathematics and Computer Science, Delft University of Technology, 2628 CD Delft, The Netherlands (e-mail: M.Popov@ieee.org).

L. Grcev is with the Faculty of Electrical Engineering and Information Technologies, Ss. Cyril and Methodius University, 1000 Skopje, Macedonia, and also with the Macedonian Academy of Sciences and Arts, 1000 Skopje, Macedonia (e-mail: Leonid.Grcev@ieee.org).

H. K. Høidalen is with the Norwegian University of Science and Technology (NTNU), 7491 Trondheim, Norway (e-mail: Hans.Hoidalen@elkraft.ntnu.no).

B. Gustavsen is with Sintef Energy, 7465 Trondheim, Norway (e-mail: Bjorn.Gustavsen@sintef.no).

V. Terzija is with the The University of Manchester, Manchester, M13 9PL, U.K. (e-mail: terzija@ieee.org).

Color versions of one or more of the figures in this paper are available online at http://ieeexplore.ieee.org.

Digital Object Identifier 10.1109/TIA.2015.2411652

I. INTRODUCTION

POWER systems are designed to produce, transmit, and distribute electricity to the remote consumers economically and in a secure manner. To achieve that, power systems are grounded at specific points. These are normally generator and transformer neutral points, which actually represent the system grounding. In this way, the ground serves as a return path for the fault currents with a resistance that should be kept as low as possible. However, it is of greatest importance that such a low ground resistance should help in decreasing the potentials during faults and other disturbances. Therefore, the goal of the grounding is twofold: 1) to provide safety against electric shock resulting from step and touch voltages for the people in the vicinity of the electrical equipment and 2) to provide the correct operation of the power system, e.g., providing the correct level of fault currents important for the operation of power system protection.

The first issue is related to the safety of the people working in the environment of the grounding system or using electrical apparatus. This is well elaborated so far [1]–[5]. In order to achieve this, substation and power plant grounding systems are usually complex grounding structures that consist of meshes in a form of horizontally interconnected conductors, which sometimes are supplied with vertical rods. The second issue, however, deals with the system grounding, and during normal power system operation, the grounding impedance is predominantly resistive and straightforward to be determined. The grounding system in this case is close to an ideal grounding, and the grounding effect can be easily included into the self- and mutual impedances of lines and cables that further determine the symmetrical component values of the transmission and distribution system [6]. However, for fast transient oscillations that occur during lightning, disconnecting lines, cables, transformers, and switchgear in GIS, the grounding system performance is quite different. Grounding impedance is frequency dependent, and in case of high intensity currents, it may be nonlinear due to earth ionization [7]. Such complex behavior of grounding systems during fast transients might enhance the overvoltages and might degrade overvoltage protection applied on the system. This effect is usually not taken into account in test laboratories that perform their test duties in a laboratory environment where equipment is grounded at one point so that the effect of the grounding is minimized.

The complex transient behavior combined with the complex geometry of the grounding structures makes the modeling of the grounding system for power system transient studies very complicated. Recently, models based on the rigorous full wave electromagnetic theory that are thoroughly tested by comparison with experiments have been described [8]–[10]. The application of these mathematically complex models is recently utilized by software with a simple graphical interface, such as TRAGSYS [10]. In this paper, we have used the TRAGSYS program to extract equivalent network parameters from the electromagnetic model of the grounding system. Such network equivalents enable a direct representation in complete system transient analysis using ATP-EMTP. The accurate computation of fast transients is very important for insulation coordination and equipment design. In this paper, it is proven that, during fast transients, the effect of the grounding system highly influences the overvoltages, which, depending on the distance between the overvoltage protection and the transformer, may exceed the basic insulation level (BIL) of the transformer.

In this paper, for the first time, we have enhanced the accuracy of computations by coupling more sophisticated models of components like transformers and lightning arresters. All models are frequency dependent, which is important for the accurate representation of the residual voltages after a lightning arrester operates. The transformer is very accurately represented so that the potentials of both the transformer and the arrester neutral point can be computed very accurately.

This paper is organized in the following way. Section II explains the approach of the complex grounding system model. Section III describes the methodology applied to interface the complex grounding system to the network. Section IV deals with the comparison of the computed results by TRAGSYS and ATP-EMTP. Section V describes the studied system and associated component modeling with a special focus on the lightning arrester model. Sections VI and VII deal with the simulated results and conclusion, respectively.

II. Modeling Complex Grounding Systems

The analysis is in the frequency domain, i.e., the response of a steady-state time-harmonic excitation computed for a wide frequency range. The interested reader may find full details on the underlying theory of the model in [8] and [9]. Here, we briefly describe the basic step in the modeling process. The physical model of the grounding system is assumed to be a network of straight cylindrical metallic conductors with arbitrary orientation. A suitable equivalent radius is assumed in the case when the conductor's cross section is not circular. It is assumed that the conductor length is much greater than the radius which is much smaller than the wavelength of the medium (in practice, the ratio of 10 is usually satisfactory). This assumption enables the so-called thin-wire approximation by which the total current in the conductors is represented by the filamentary line current in the conductors' axis. We consider the grounding system detached from the above ground system and completely buried in the earth. In the present analysis, we assume a homogenous model of soil characterized by apparent conductivity and permittivity constants. The case in which the soil is layered with different characteristics of layers will be considered in later work.

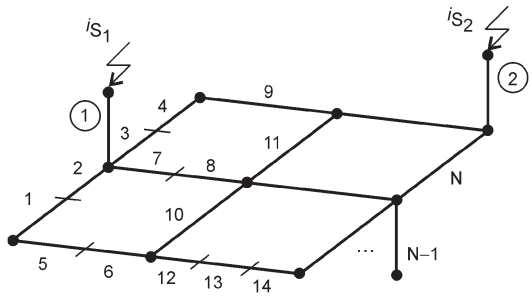

Fig. 1. Grounding system model divided into fictitious segments.

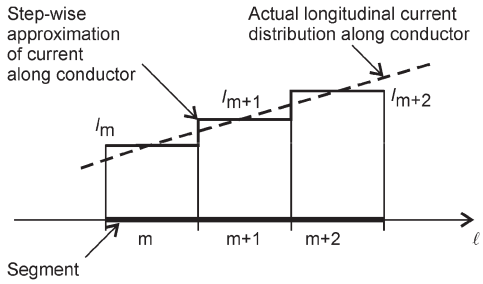

Fig. 2. Actual longitudinal current distribution along conductor axis and its stepwise approximation.

The basic goal of the modeling is to determine the longitudinal current distribution along conductors in the grounding system. The first step in the analysis is to divide the grounding conductors into fictitious segments (all segments must be subject to thin-wire approximation). Fig. 1 illustrates such a division in fictitious segments. They can have variable length which is numbered appropriately. We distinguish segments with open ends in which a current is injected. These segments are numbered by $m = 1, 2, \ldots, M$ and shown with encircled numbers in Fig. 1. All the other segments are numbered separately by $n = 1, 2, \ldots, N$. The next step is to assume a longitudinal current distribution along a segment. The simplest approximation is to assume a constant distribution [8]. Another possibility for the approximation of the current along segments is described in [9]. In such a case, the current along the nth segment is

$$I(l) = I_n F_n(l) \tag{1}$$

where $F_n(l)$ is equal to one for the nth segment and zero elsewhere. Here, I_n is the phasor that determines the current at the nth segment.

Therefore, the current distribution along conductors' length l is approximated by a stepwise approximation

$$I(l) = \sum_{n=1}^{N} I_n F_n(l). \tag{2}$$

The goal of this analysis is to determine the unknown I_n. Fig. 2 illustrates the actual longitudinal current and its stepwise approximation.

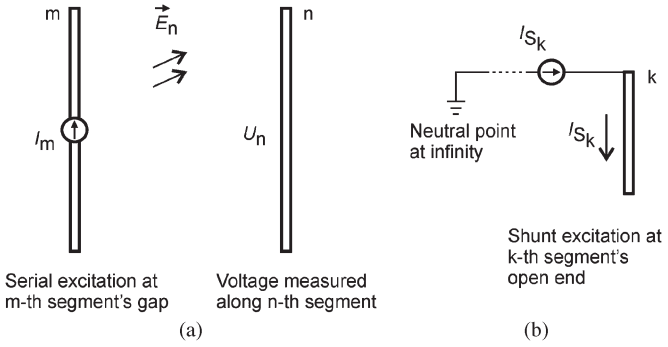

Fig. 3. (a) Interaction between segments with serial excitation. (b) Segment with shunt excitation.

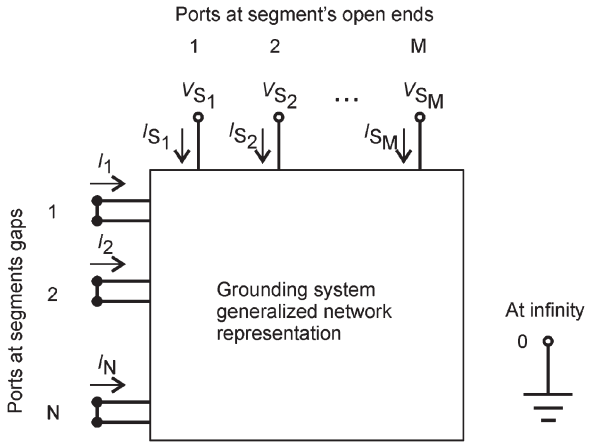

Fig. 4. Generalized network representation of the grounding system.

Since the current flows from the conductors into the soil, the longitudinal current is variable along the conductors. It is clear that the accuracy of the approximation depends on the total number of segments, N; larger number (and smaller) segments lead to an increased accuracy. The next step is to determine the electromagnetic interaction between segments. Here, we distinguish M segments with shunt excitation (by the injection of current) and the other N segments that can have serial excitation. We assume that such serial excitation can be applied by an ideal current or voltage generator connected between infinitesimal gaps at the segment center. Therefore, we assume that there exists a two-terminal port at the center of the segment, which is short-circuited when there is no serial excitation. First, we consider two segments with a serial excitation and denote them by "m" and "n" in Fig. 3(a). If an ideal current generator with a current I_m is applied, a constant current is impressed along the nth segment. Next, we can determine the resulting electric field $\vec{E}_n$ at the surface along the nth segment. The induced voltage U_n along the nth segment is obtained by integrating the tangential component of $\vec{E}_n$. The electromagnetic interaction between the segments is determined by the generalized impedances [11]

$$z_{mn} = \frac{U_n}{I_m}, \qquad n = 1, 2, \ldots, N, \quad m = 1, 2, \ldots, N. \tag{3}$$

Similarly, the mutual impedance between a segment with a shunt excitation (current injection) and another segment is

$$z'_{mn} = \frac{U_n}{I_{S_m}}, \qquad n = 1, 2, \ldots, N, \quad m = 1, 2, \ldots, M. \tag{4}$$

This is equivalent to a network representation of the grounding system where N two-terminal ports are at the infinitesimal gaps at the segments' center while M one-terminal ports correspond to segments where current injection is applied (the other terminal of these ports is at a neutral point—theoretically at infinity); see Fig. 4. Segment gap ports are short-circuited in the normal operation, but they can be used to simulate impressed serial excitation when the grounding structure is under the influence of an external field. We consider that the grounding system excitation consists of M ideal current generators with currents $I_{S_k}, k = 1, 2, \ldots, M$ connected between the one-terminal ports and the neutral point at infinity (the influence of the connecting cables is neglected). Based on the linearity and the superposition principle, the interaction between all segments is described by the following matrix equation [12]:

$$\begin{bmatrix} z_{11} & z_{12} & \cdots & z_{1N} \\ z_{21} & z_{22} & \cdots & z_{2N} \\ \vdots & \vdots & \ddots & \vdots \\ z_{N1} & z_{N2} & \cdots & z_{NN} \end{bmatrix} \cdot \begin{bmatrix} I_1 \\ I_2 \\ \vdots \\ I_N \end{bmatrix} = \begin{bmatrix} z'_{11} I_{S_1} + z'_{12} I_{S_2} + \cdots + z'_{1M} I_{S_M} \\ z'_{21} I_{S_1} + z'_{22} I_{S_2} + \cdots + z'_{2M} I_{S_M} \\ \vdots \\ z'_{N1} I_{S_1} + z'_{N2} I_{S_2} + \cdots + z'_{NM} I_{S_M} \end{bmatrix}. \tag{5}$$

The solution of (5) provides the coefficients I_m for N segments

$$[I] = [z]^{-1} \cdot \{I_{S_1}[z'_1] + I_{S_2}[z'_2] + \cdots + I_{S_M}[z'_M]\} \tag{6}$$

and, therefore, the longitudinal current distribution (2) along all conductors of the grounding system. When the currents are known, all other quantities of interest, such as fields, potentials, voltages, and impedances, can be straightforwardly computed.

III. Interface to Transient Programs

The M ports at segments' open ends are connecting points to the power system. The interface to the power system is based on impedances seen from and between these M ports. The self- and the mutual grounding harmonic impedance seen from and between M ports at segment open ends are

$$Z_{S_{mn}} = \frac{V_{S_m}}{I_{S_n}} = \frac{[I]^T [z'_n] + I_{S_n} z'_{S_{mn}}}{I_{S_n}}, \qquad m = 1, 2, \ldots, M, \quad n = 1, 2, \ldots, M. \tag{7}$$

All quantities to determine $Z_{S_{mn}}$ in (7) are already evaluated by (6), except $z'_{S_{mn}}$, which are mutual impedances between shunt excitation segments "m" and "n."

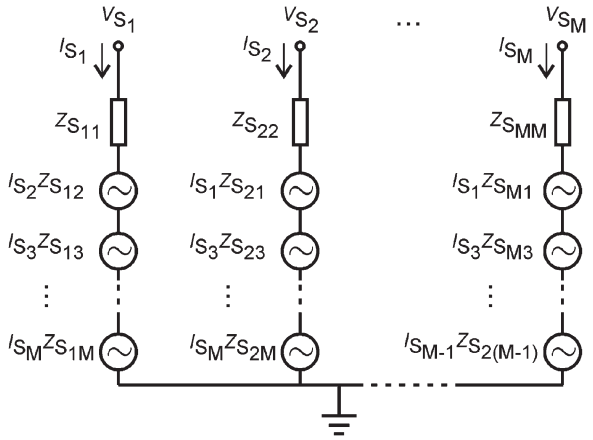

Fig. 5. Grounding system equivalent circuit seen from the above ground power system.

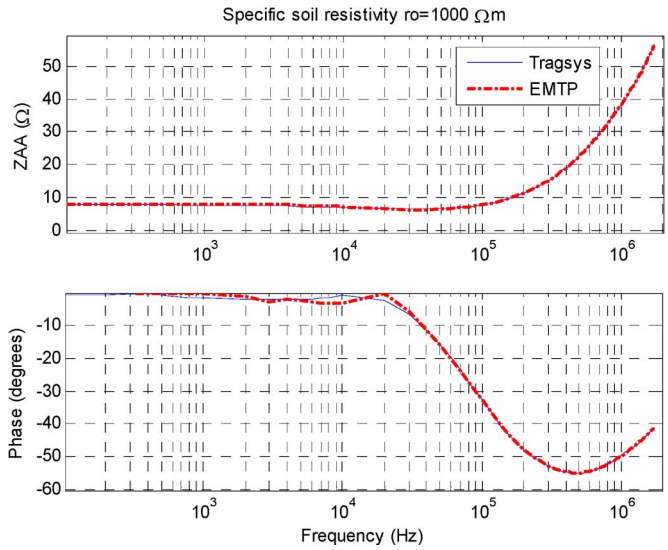

Fig. 6. Amplitude and phase characteristic of the impedance Z_{AA} at the arrester grounding point of the grounding system, for the soil resistivity of 1000 Ωm.

Therefore, we have reduced the order of the network representation of the grounding system from $N + M$ in (5) to M

$$[V_S] = [Z_S] \cdot [I_S]. \tag{8}$$

The equivalent circuit seen from the above grounding system is illustrated in Fig. 5. The next step is to approximate $Z_{S_{mn}}$ represented by a linear approximation by a vector fitting procedure and/or Armafit. Transient programs like ATP-EMTP are capable of dealing with circuits such as those presented in Fig. 5. By making use of the powerful user-defined Tacs/Models, current-controlled voltage sources are programmed in Models, whereas the self-impedance is synthesized and applied directly in ATP-EMTP.

In order to represent the grounding system accurately, the impedances from (8) need to be fitted within a broad frequency range. So far, there was a lot of work done on synthesizing frequency-dependent characteristics by electric circuits. In [13], an efficient method to represent the impedance characteristic within a broad frequency range was provided. This is valid only for self-impedances.

There were different methods investigated to find the most appropriate way of representing these impedances. It was found that the self-impedances of $Z_{S_{mn}}$ fitted by making use of the Armafit approach [14], [15] are very efficient to represent the impedance within a broad frequency range. Moreover, this approach provides the coefficients of a rational function known as Kizilcay F-dependent [16], which is directly implementable in ATP-EMTP environment. Off-diagonal impedances are fitted by making use of the vector fitting approach [17]. In this way, the fitting of the characteristics is obtained with high accuracy. Furthermore, the off-diagonal elements are expressed in partial fractions since they need to be multiplied by the current that is provided from the power system simulated in ATP-EMTP. As an output, the computed voltage is provided, which is exported to a type-60 current-controlled voltage source. The fitted characteristics are expressed by

$$Z_{S_{mn}}(s) = D + sE + \sum_{n=1}^{N_p} \frac{\underline{c}_n}{s - \underline{a}_n} \tag{9}$$

where N_p is a positive integer, $s = j\omega.D$ and E are real, whereas $\underline{c}_n$ and $\underline{a}_n$ could be either real and/or a pair of complex conjugated numbers, which can be represented as a second-order polynomial partial fraction with real constant parameters. In this way, it is possible to represent the expressions in Models by making use of the Laplace function. Alternatively, the fitting of the whole matrix $Z(s)$ can be done by vector fitting. The use of both gives an opportunity to use also embedded models of ATP-EMTP like Kizilcay F-dependent.

IV. Model Validation

A. Validation of the Computed Impedance Characteristics

The previously described procedure is applied on a grounding system with dimensions of 60 m × 60 m. In this case, the impedance characteristics dependent on frequency are determined by the electromagnetic model and fitted accordingly. Fig. 6 shows the results of the synthesized characteristics for a feeding point at the lightning arrester location AA. For this case, a lightning impulse of 10 kA and 1.2/50 μs has been injected at AA, and the corresponding voltage has been computed. Fig. 7 shows the results of the ground potential rise at the same point where the current is injected. It can be seen that the ATP-EMTP model shows very good matching with the electromagnetic model.

Figs. 8 and 9 show the results for a case when the lightning occurs at the point M located in the middle of the grounding system. Fig. 8 is the impedance characteristic of the grounding system seen from the point M for a specific soil resistivity of 1000 Ωm.

Fig. 9 shows the corresponding ground potential rise when a lightning stroke is injected in the middle of the grounding systems.

Figs. 10 and 11 present the results of the mutual impedance characteristics between the arrester grounding point and the middle point, and the corresponding ground potential rise.

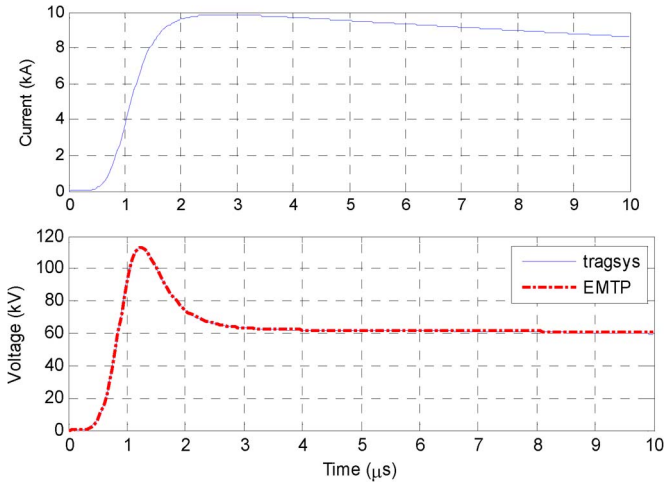

Fig. 7. Current impulse of 1.2/50 μs and corresponding ground potential rise at the arrester grounding point.

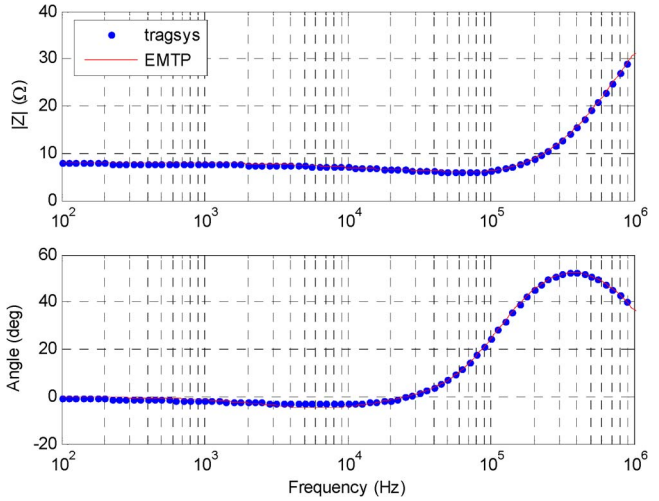

Fig. 8. Amplitude and phase characteristic of the impedance Z_{MM} in the middle of the grounding system.

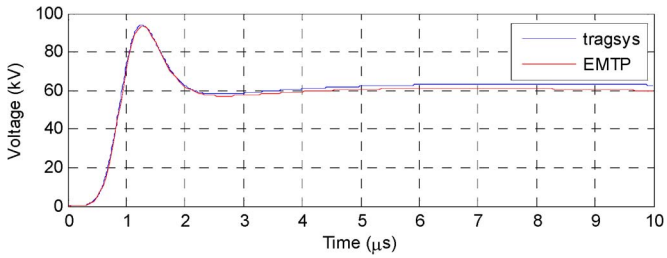

Fig. 9. Ground potential rise in the middle of the grounding system.

Fig. 11 shows the voltage rise at the arrester earthing point when the lighting is injected in the middle point of the grounding system. It can be seen that the last case differs significantly with respect to the previous case. The voltage rise is delayed by approximately half of a microsecond.

Accordingly, the impedance characteristics are fitted for a specific resistivity of 100 Ωm, and time domain voltage responses are verified in the same way.

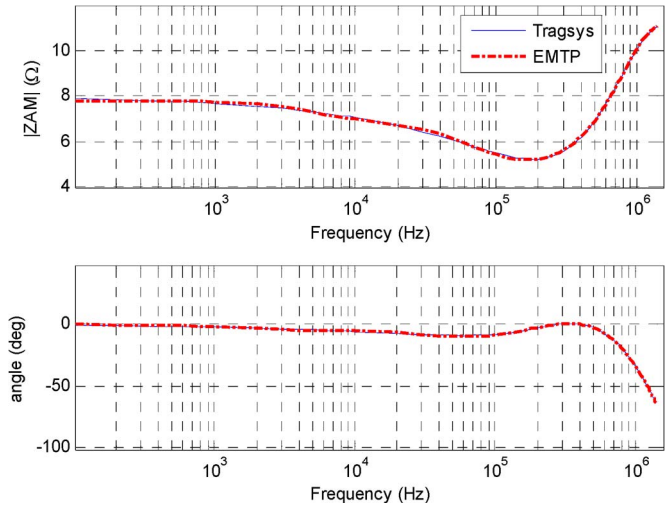

Fig. 10. Amplitude and phase characteristic of the mutual impedance Z_{AM} between the arrester earthing point AA and the middle point MM of the grounding system for a specific soil resistivity of 1000 Ωm.

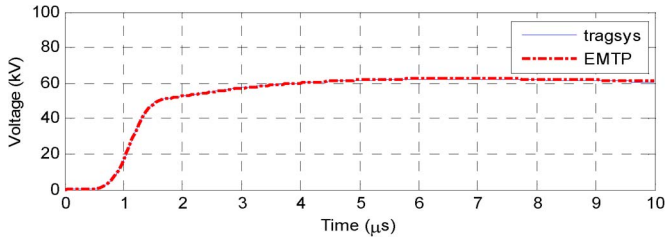

Fig. 11. Ground potential rise at the arrester grounding point when the lightning stroke is injected in the middle point of the grounding system.

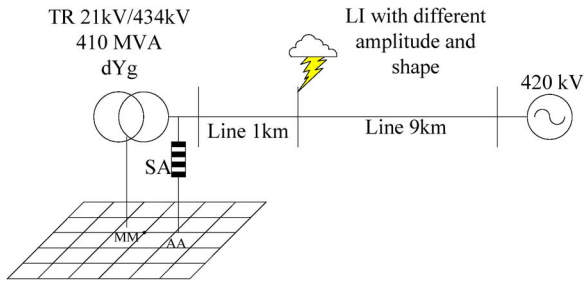

Fig. 12. Illustration of the studied system.

V. Studied System

The analysis is performed for a 420-kV network as illustrated in Fig. 12. The system consists of an overhead line connecting a 434/21-kV power transformer with a BIL of 1425 kV. The transformer is protected by lightning arresters installed 15 m away from the transformer. The grounding system is a 60 m × 60 m grid consisting of 10 m × 10 m meshes constructed from copper conductors with a diameter 1.4 cm, buried at a 0.5-m depth. The soil is homogeneous with a resistivity of 100 Ωm, relative permittivity of 10, and permeability of air.

The overhead line is modeled by ATP's J-Marti frequency-dependent transmission line model. The 15-m connection between the lightning arresters and the transformer is also

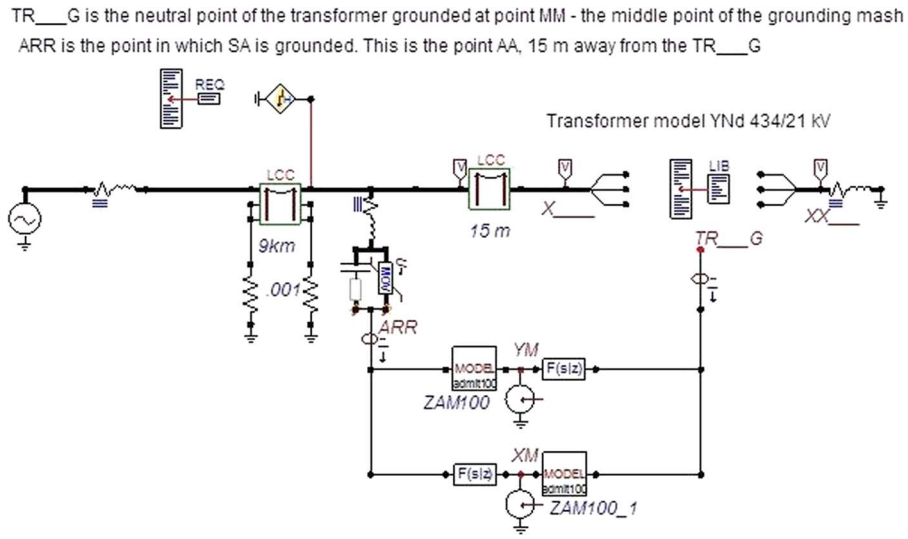

Fig. 13. Representation of the studied system modeling in ATPDraw.

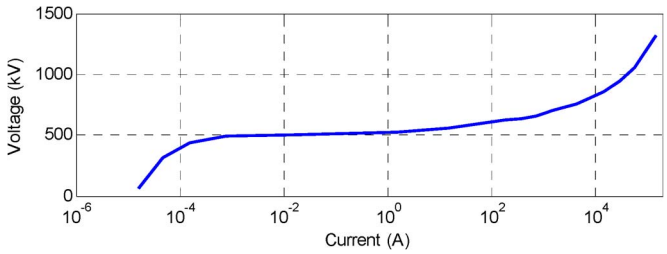

Fig. 14. Lightning arrester characteristic.

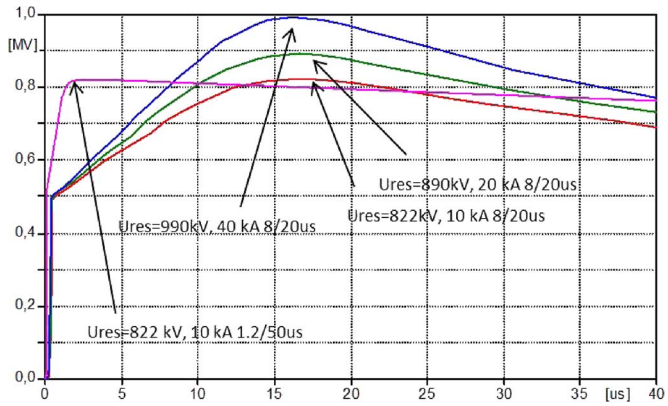

Fig. 15. Results of the residual voltages for different wave shapes.

modeled by the J-Marti routine. Refined models for the lightning arresters and the transformer are applied as detailed in the following sections. All models are implemented in ATPDraw environment as shown in Fig. 13. The overhead line consists of two conductors per phase and is equipped with ground wires. In this paper, we consider a worst case scenario with the lightning strike directly on phase wires without any flashover along the line. Ground wires in this case are also not connected to the studied grounding system.

A. Lightning Arrester Modeling

The choice of the lightning arrester is made according to the nominal system voltage and the corresponding maximum continuous operating voltage U_c. Moreover, it is also recommended to pay attention to the line discharge class, which is related to the absorbed arrester energy. According to [19], a PEXLIM Q arrester of class 3 with 7.8 kJ/kV and with rated and continuous operating voltages $U_r = 336$ kV and $U_c = 267$ kV has been chosen. The U–I characteristic for this arrester is determined by making use of [20] and is shown in Fig. 14.

For high frequencies corresponding to impulses with a short front of wave, however, the variable resistance computed according to Fig. 14 is not enough. Therefore, a frequency-dependent arrester model is applied [21]. The nonlinear resistance computed from Fig. 14 is connected in parallel with a capacitor of 0.3 nF, and this parallel connection is connected in series with an R-L branch of 1 mΩ and 1 μH. With these data, satisfactory results can be achieved, which are close to the catalog data. Fig. 15 summarizes the results of the applied model for different impulses. For 10, 20, and 40 kA with a waveform of 8/20 μs, the model results in 820, 890, and 990 kV, respectively. These values are slightly higher than those provided in the catalog, which are 790, 869, and 972 kV. For an impulse of 10 kA and 1.2/50 μs, the computed value is 822 kV. These data are not provided in the catalog, but the experience shows that the voltage is 5%–8% higher than that with an impulse of 8/20 μs, which, in this case, results between 830 and 855 kV.

B. Transformer Modeling

The transformer is represented by a frequency-dependent model of the form (9). The model is obtained from frequency sweep measurements of the 6 $\times$ 6 transformer terminal admittance which are subjected to model extraction using vector fitting and passivity enforcement. More details about the modeling of this transformer and the model performance can be found in [22]. The model is included in ATP-EMTP environment

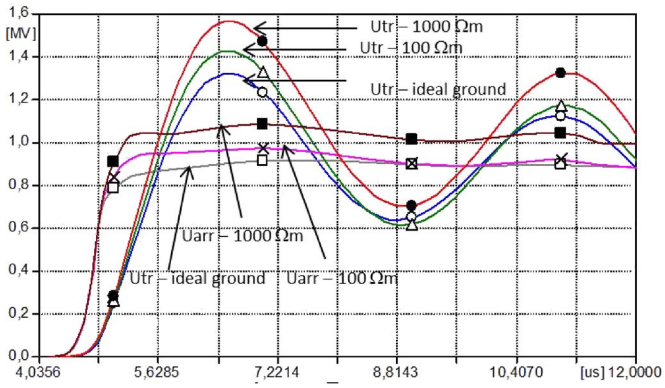

Fig. 16. Comparison between transformer voltages for different specific soil resistivity and ideal grounding for a discharge current of 25 kA and 1.2/50 μs.

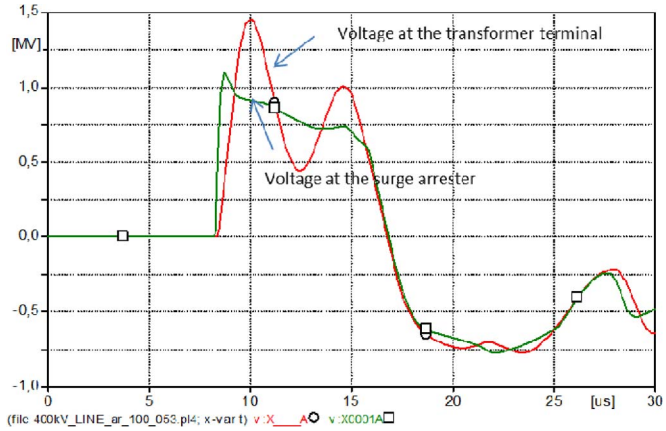

Fig. 17. Voltage response when the system is exposed to LI of 0.5/3 μs and 30 kA and soil resistivity of 100 Ωm.

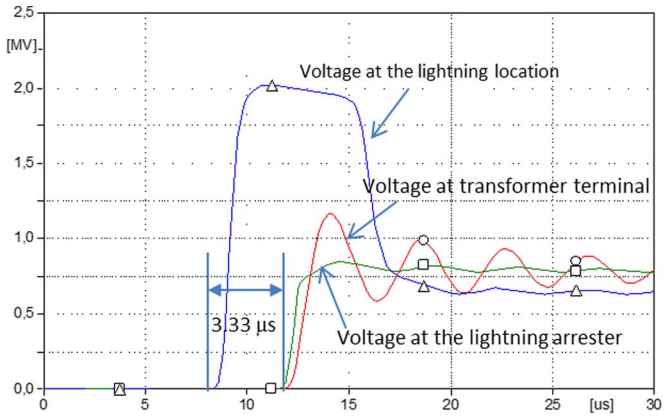

Fig. 18. Overvoltages on the lightning arrester and transformer terminals when the lightning of 10 kA and 1.2/50 μs occurs at 1-km distance from the transformer.

using an equivalent electrical circuit which is generated directly from the pole-residue model.

Although the measurements were only available up to 200 kHz, the transformer model will, in this work, be used in an application involving higher frequencies. This could slightly affect the final results; however, more measurements about the transformer at the time when this work was done could not be provided. On the other hand, the surged voltages strongly depend on the rest of the network and especially the calculated residual voltages of the lightning arrester as well as the impedance terminal characteristic of the grounding system itself [23], which, in this work, are provided with great accuracy as previously described.

VI. Results

Based on the performed modeling and system data, an extensive analysis has been carried out in order to see how different lightning impulses affect the lightning arrester with respect to the generated overvoltages. It is also paid attention to see the effect of different values of specific soil resistivity as well as under which conditions the terminal transformer voltage exceeds the transformer BIL. For all cases, the lightning arrester distance from the transformer is kept fixed at 15 m. A change of this parameter implies that the new value of Z_{AA} and Z_{AM} should be recomputed and included. This is not done because it is actually known that the longer the distance between the lightning arrester and transformer, the higher the overvoltages [5]. Moreover, the neutral points of the lightning arresters for all three phases in this study are considered grounded in one point. This is done for two reasons. The first reason is that only two current injections from the power system are applied (the transformer grounding and the arrester grounding), which requires fewer characteristics to be included.

This simplifies the computation procedure, which, even with two current injection points, is rather complicated. The second reason is that these points, in practice, will be very close to each other and will result in low impedances, which do not change the ground potential rise and terminal arrester voltages very much. The performed analysis shows that, for the selected grounding system, the specific resistivity plays an important role. Fig. 16 shows that, when the grounding is considered as ideal, for a discharge current of 25 kA and 1.2/50 μs, the transformer terminal voltage is about 1.3 MV and the arrester terminal voltage is around 900 kV. However, when the specific resistivity is 100 Ωm and 1000 Ωm, transformer terminal voltages rise above 1.4 MV, exceeding the transformer BIL. The residual arrester voltages rise accordingly, and this is caused by the higher ground potential rise of the arrester grounding point. Fig. 17 shows an example when the system is exposed to a lightning with 30 kA and a front of wave of 0.5 μs, which is shorter than that in the previous case. In this case, the tail of the lightning impulse is 3 μs, which is much shorter than that in the previous case. It can be seen that, for a specific resistivity of 100 Ωm, this case results in a transformer overvoltage much higher than the transformer BIL. These examples and the rest of the examples of the performed study deal with lightning strokes *that take place at the lightning arrester*, very close to the substation where the transformer is located. However, one should be aware that overvoltages that propagate along the lines are much higher than these values. This is demonstrated in Fig. 18, which shows the result of a case when the lightning occurs 1 km away from the arrester location. This example demonstrates the traveling wave phenomena and worst case scenario; it is considered that the lightning hits the phase

TABLE I
COMPUTED RESULTS FOR A LI OF 1.2/50 μs

R (Ωm)	Is (kA)	Iarr (kA)	Uarr (kV)	Utr(kV)
100	10	9.46	846	1170
100	20	20.2	935	1355
100	25	25.4	973	1425
1000	10	10	874	1226
1000	20	20.2	1025	1464
1000	25	25.2	1084	1566

TABLE II
COMPUTED RESULTS FOR A LI OF 0.5/3 μs

R (Ωm)	Is (kA)	Iarr (kA)	Uarr (kV)	Utr(kV)
100	10	5.6	800.7	1157
100	20	13	948	1324
100	25	17.5	1030	1388
1000	10	5.6	844	1184
1000	20	12.5	1115	1395
1000	25	17.1	1232	1484

TABLE III
COMPUTED RESULTS FOR A LI OF 0.5/50 μs

R (Ωm)	Is (kA)	Iarr (kA)	Uarr (kV)	Utr(kV)
100	10	10	844	1194
100	20	20	949	1368
100	25	25	1029	1433
1000	10	9.9	888	1238
1000	20	20	1076	1468
1000	25	25	1181	1568

TABLE IV
COMPUTED RESULTS FOR A LI OF 4/10 μs

R (Ωm)	Is (kA)	Iarr (kA)	Uarr (kV)	Utr (kV)
100	20	18.2	918	1091
100	50	46.7	1112	1243
100	100	96.2	1381	1415
1000	20	18.2	998	1163
1000	50	46.4	1316	1405
1000	100	95.3	1810	1805

conductors (even though the line is supplied by ground wires). The possible flashover because of the very high overvoltage is also not taken into account.

Since the speed of wave propagation in overhead lines is close to the speed of light, the wave travel time from the place where the lightning occurs to the lightning arrester terminals is $1\ \text{km}/3e5\ \text{km/s} = 3.3\ \mu\text{s}$. Within this very short period of time, the overvoltage rises to a very high value, which, in this case, is around 2 MV. Upon reflection from the lightning arrester, the voltage is surged to a value of approximately 830 kV, which corresponds well to the residual voltage of the catalog data. It can be seen that the voltage at the transformer terminals starts rising shortly after the arrester terminals are reached. This is approximately 50 ns, which is equal to the wave travel time from the arrester terminals to the transformer terminals. Tables I–IV summarize the results of the computed overvoltages at the arrester and transformer terminals for different specific soil resistivities and lightning currents as well as different lightning wave shapes. It can be seen that longer tails of the lightning impulses result in more discharge arrester current. Moreover, in all cases, for a particular lightning impulse, higher specific soil resistivity results in higher transformer terminal

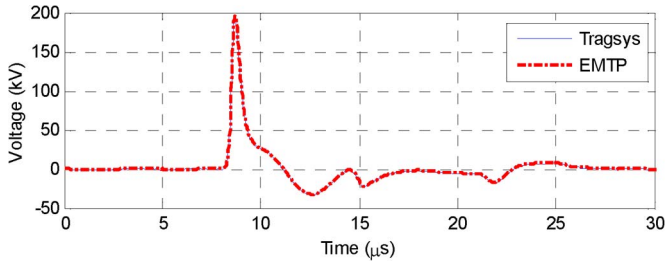

Fig. 19. Voltage at the arrester grounding point AA computed by TRAGSYS and EMTP for the case of lighting current of 30 kA and 0.5/3 μs and soil resistivity of 100 Ωm.

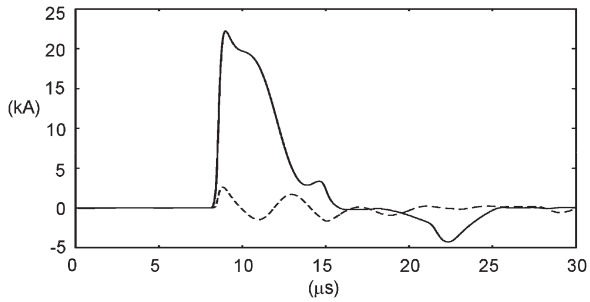

Fig. 20. Current injected into the grounding system for the case of lighting current of 30 kA and 0.5/3 μs and soil resistivity of 100 Ωm. Full line—At arrester grounding point. Broken line—At transformer.

overvoltage. For lightning impulses for which front times are longer, BIL is even not achieved when the lightning current is 50 kA. However, higher specific resistivity significantly influences the residual voltage of the lightning arrester. For example, according to Table I, for a lighting current of 25 kA and specific resistivities of 100 Ωm and 1000 Ωm, the residual voltages of the lightning arrester are 973 and 1084 kV, respectively. This can be well seen in Fig. 16. The difference of the residual voltage also affects the terminal transformer overvoltages, which, in this case, for both values of the soil resistivity, exceed the predefined transformer BIL.

The discharge current through the lightning arresters is large when the arrester operates and causes high ground potential rise. Fig. 19 shows a comparison between the ground potential rise computed by TRAGSYS and ATP-EMTP. This is also a verification that the interface of the whole grounding system is well done in ATP-EMTP environment.

Fig. 20 shows the currents injected into the grounding system for the case of a lighting current of 30 kA and 0.5/3 μs and a soil resistivity of 100 Ωm at the arrester and at transformer grounding points. These currents are used to analyze the potential distribution in the ground as shown in Fig. 21. The resulting temporal and spatial distribution of the potential of ground grid conductors is presented as individual "snapshots" of the computer animation. It can be seen that, in the first instants of the current injection in the grounding system, due to the limited speed of propagation, only a smaller part of the grounding system is active in discharging current into soil, which results in very large potentials near the injection point. The complex propagation of potentials and induced voltages during the transient period computed by the described method are of interest in electromagnetic compatibility (EMC) studies of connected sensitive equipment.

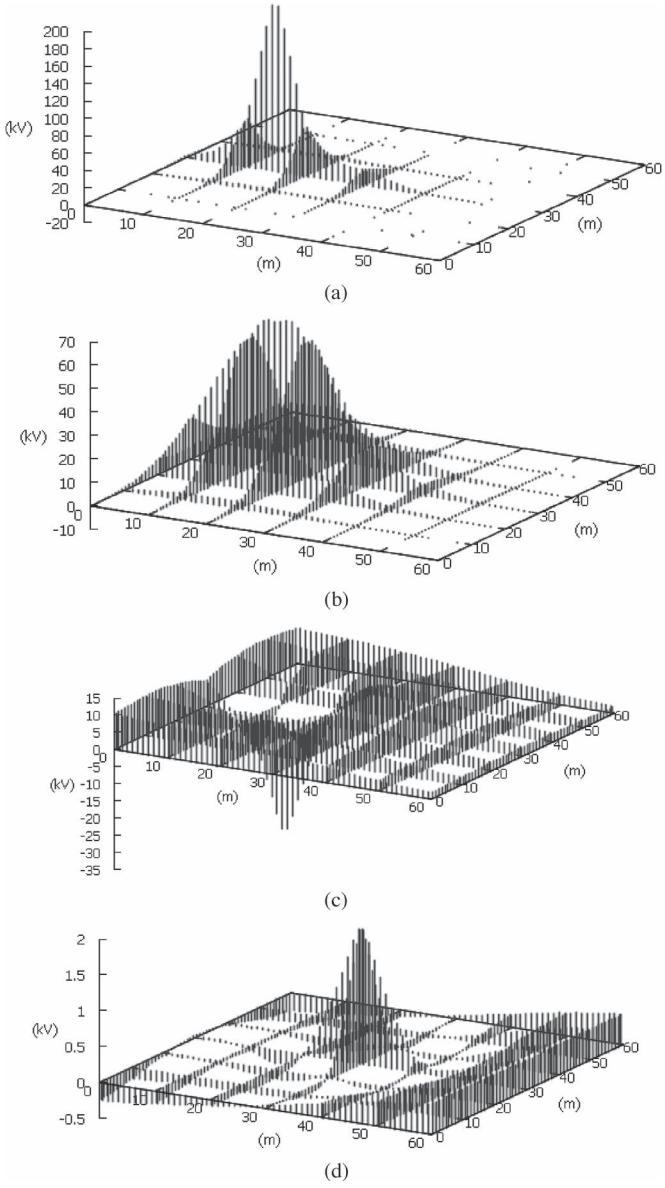

Fig. 21. Snapshots of computer animation of the potential distribution at grounding conductors computed by TRAGSYS for the case of lighting current of 30 kA and 0.5/3 μs and soil resistivity of 100 Ωm. (a) $t = 8.7$ μs. (b) $t = 9.2$ μs. (c) $t = 12.6$ μs. (d) $t = 30$ μs.

VII. Conclusion

This paper has presented a very accurate study of a complex grounding system behavior when large transformers are exposed to severe lightning conditions. It has been shown that the grounding impedance that depends on the grounding mesh structure and the soil resistivity plays an important role in the determination of the correct overvoltage values. This paper also demonstrates an efficient interface that is built in ATPDraw environment and is based on a proven methodology. According to this methodology, when the connection points of the system above ground are known and the self- and mutual impedances for the predefined grounding system from these points are determined, the grounding system can be interfaced to the system above ground with full success. Ignoring grounding resistances and considering the earth as an ideal conductor, or predicting constant values for the grounding resistance may lead to very inaccurate results even though the system components above ground are modeled within a broad frequency range. More work will be done in the future to show the effect of the grounding system when the lightning hits the overhead line ground wires (if they exist), and what the overvoltage values will be in case when a flashover takes place between overhead line conductors. This will require an extended application of this methodology that will take into account ground wires earthing.

References

[1] *Guide for Safety in AC Substation Grounding*, IEEE Std. 80-2000, 2000.
[2] M. Mitolo, "Of electrical distribution systems with multiple grounded neutrals," *IEEE Trans. Ind. Appl.*, vol. 46, no. 4, pp. 1541–1546, Jul./Aug. 2010.
[3] M. Mitolo, "Grounding the neutral of electrical systems through low-resistance grounding resistors: An application case," *IEEE Trans. Ind. Appl.*, vol. 44, no. 5, pp. 1311–1316, Sep./Oct. 2008.
[4] F. Freschi, A. Guerrisi, M. Tartaglia, and M. Mitolo, "Numerical simulation of heart-current factors and electrical models of the human body," *IEEE Trans. Ind. Appl.*, vol. 49, no. 5, pp. 2290–2299, Sep./Oct. 2013.
[5] ABB. [Online]. Available: http://www.abb.com/product/db0003db004279/c125739900636470c125708c0041b9a9.aspx
[6] J. J. Grainger and W. D. Stevenson, *Power System Analysis*, McGraw-Hill International Edition. New York, NY, USA: McGraw-Hill, 1994.
[7] E. D. Sunde, *Earth Conduction Effects in Transmission Systems*. New York, NY, USA: Dover, 1968.
[8] L. Grcev and F. Dawalibi, "An electromagnetic model for transients in grounding systems," *IEEE Trans. Power Del.*, vol. 5, no. 4, pp. 1773–1781, Oct. 1990.
[9] L. Grcev, "Computer analysis of transient voltages in large grounding systems," *IEEE Trans. Power Del.*, vol. 11, no. 2, pp. 815–823, Apr. 1996.
[10] TRAGSYS-Software for High Frequency and Transient Analysis of Grounding Systems. [Online]. Available: http://www.tragsys.com
[11] R. F. Harrington, *Field Computation by Moment Methods*. New York, NY, USA: Wiley-IEEE Press, 1993.
[12] M. Heimbach and L. Grcev, "Grounding system analysis in transients programs applying electromagnetic field approach," *IEEE Trans. Power Del.*, vol. 12, no. 1, pp. 186–193, Jan. 1997.
[13] L. Grcev and M. Popov, "On high-frequency circuit equivalents of a vertical ground rod," *IEEE Trans. Power Del.*, vol. 20, no. 2, pp. 1598–1603, Apr. 2005.
[14] T. Noda and N. Nagaoka, "Development of ARMA models for transient calculation using linearized least-square method," *Trans. Inst. Elect. Eng. Trans. Jpn.*, vol. 114-B, no. 4, pp. 396–402, 1994.
[15] T. Noda, N. Nagaoka, and A. Ametani, "Phase domain modeling of frequency transmission lines by means of an ARMA model," *IEEE Trans. Power Del.*, vol. 11, no. 1, pp. 401–411, Jan. 1996.
[16] M. Kizilcay, "Low-order network equivalent for electromagnetic transient studies," *Eur. Trans. Elect. Power Eng.*, vol. 3, no. 2, pp. 123–129, Mar./Apr. 1993.
[17] B. Gustavsen and A. Semlyen, "Rational approximation of frequency domain responses by vector fitting," *IEEE Trans. Power Del.*, vol. 14, no. 3, pp. 1052–1061, Jul. 1999.
[18] B. Gustavsen, "Computer code for rational approximation of frequency dependent admittance matrices," *IEEE Trans. Power Del.*, vol. 17, no. 4, pp. 1093–1098, Oct. 2002.
[19] ABB Surge Arresters—Buyers Guide, 5.1 ed., ABB, Zurich, Switzerland, Apr. 2007.
[20] [Online]. Available: http://www.arresterworks.com/
[21] M. Popov, L. van der Sluis, and G. C. Paap, "Investigation of the circuit breaker reignition overvoltages caused by no-load transformer switching surges," *Eur. Trans. Elect. Power*, vol. 11, no. 6, pp. 413–422, 2001.
[22] B. Gustavsen, A. P. Brede, and J. O. Tande, "Multivariate analysis of transformer resonance overvoltages in power station," *IEEE Trans. Power Del.*, vol. 26, no. 4, pp. 2563–2572, Oct. 2011.
[23] C. L. Bak *et al.*, "Overvoltage protection of large power transformers—A real-life study case," *IEEE Trans. Power Del.*, vol. 23, no. 2, pp.657–666, Apr. 2008.

Marjan Popov (M'95–SM'03) received the Dipl.-Ing. degree from the Ss. Cyril and Methodius University, Skopje, Macedonia, in 1993 and the Ph.D. degree in electrical power engineering from the Delft University of Technology (TU Delft), Delft, The Netherlands, in 2002.

He is currently an Associate Professor of electrical power engineering at TU Delft. His research interests are large-scale power system transients, intelligent protection for power systems, and wide area monitoring and protection. He is a member of CIGRE (International Council on Large Electric Systems) and Dutch national SC B5 and actively participated in CIGRE JWG C4.402 and JWG A2/C4.39 as well as CIGRE JWG A2/C4.52.

Prof. Popov received the prestigious Dutch Hidde Nijland award in 2010 for extraordinary research achievements in the field of electrical power engineering in The Netherlands. He is also a recipient of the IEEE PES Prize Paper Award and IEEE Switchgear Committee Award in 2011.

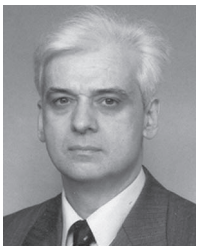

Leonid Grcev (M'84–SM'97–F'13) received the Dipl.-Ing. degree in electrical engineering from the Ss. Cyril and Methodius University, Skopje, Macedonia, in 1978 and the M.S. and Ph.D. degrees in electrical engineering from the University of Zagreb, Zagreb, Croatia, in 1982 and 1986, respectively.

Currently, he is a Professor with the Faculty of Electrical Engineering and Information Technologies, Ss. Cyril and Methodius University, Skopje, Macedonia, where he has been since 1988. From 1978 to 1988, he was with the Electric Power Company of Macedonia. He has been a Visiting Professor at the Technical University of Aachen, Aachen, Germany, Eindhoven University of Technology, Eindhoven, The Netherlands, and the Swiss Federal Institute of Technology, Lausanne, Switzerland. He is the principal author of the TRAGSYS software for transient analysis of grounding systems.

Prof. Grcev is a member of the Macedonian Academy of Sciences and Arts.

Hans Kr. Høidalen (M'05–SM'14) was born in Norway in 1967. He received the M.Sc. and Ph.D. degrees from the Norwegian University of Science and Technology, Trondheim, Norway, in 1990 and 1998, respectively.

He is currently a Professor at the Norwegian University of Science and Technology. His interests include power system transients, lightning, and electrical stress calculations. In recent years, his focus has been on transformer analysis and power system protection. He is the developer of the preprocessor to EMTP-ATP called ATPDraw.

Bjørn Gustavsen (M'94–SM'03–F'14) was born in Norway in 1965. He received the M.Sc. degree and the Dr. Ing. degree in electrical engineering from the Norwegian Institute of Technology, Trondheim, Norway, in 1989 and 1993, respectively.

Since 1994, he has been with SINTEF Energy Research, Trondheim, where he is currently the Chief Scientist. His research interests include the simulation of electromagnetic transients and modeling of frequency-dependent effects. He spent 1996 as a Visiting Researcher at the University of Toronto, Toronto, ON, Canada, and the summer of 1998 at the Manitoba HVDC Research Centre, Winnipeg, MB, Canada. He was a Marie Curie Fellow at the University of Stuttgart, Stuttgart, Germany (August 2001–August 2002). He is a convenor of CIGRE (International Council on Large Electric Systems) JWG A2/C4.52.

Vladimir Terzija (M'95–SM'00) received the Dipl.-Ing., M.Sc. and Ph.D. degrees in electrical power engineering from the University of Belgrade, Serbia, in 1988, 1993, and 1997, respectively.

He is the The Engineering and Physical Sciences Research Council (EPSRC) Chair Professor in Power System Engineering in the School of Electrical and Electronic Engineering, The University of Manchester, Manchester, U.K., where he has been since 2006. From 1997 to 1999, he was an Associate Professor at the University of Belgrade, Serbia. In 1999, he was awarded a Humboldt Research Fellowship. From 2000 to 2006, he was with ABB, Germany, working as an expert for switchgear and distribution automation. His main research interests are applications of intelligent methods to power system monitoring, control, and protection, switchgear and fast transient processes, and DSP applications in power.